PATCH ANTENNA ANALYSIS BASED ON RESONATOR MODEL

Jelena Šoškić[*], *Budimir Lutovac*[**] , *Dragan Filipović* [***]

Keywords: *Patch antenna, Resonator model, Radiation pattern*

Abstract: This paper presents an analysis of the rectangular patch antenna. The analysis is based on the resonator model. Theoretical results are verified by using the software package MATLAB. Besides, some of the patch antenna parameters, which are very important for design and analysis of patch antennas, are presented in the same program package.

1. INTRODUCTION

The patch antenna is a very simple radiating structure which can be realized in printed technique. It is designed as a single-layer structure and consists of four parts: patch, ground plane, substrate and the feeding part.

The patch is a very thin metal strip located on one side of a thin, non conducting substrate. The patch is normally made of thin copper foil plated with a corrosion resistive metal, such as gold, tin, or nickel.

Many shapes of patches are designed, the most popular being rectangular and circular.

A rectangular patch antenna is shown in Fig. 1.

[*] Jelena Šošlić (corresponding author) is with the Faculty of Electrical Engineering, University of Montenegro, Montenegro (e-mail: jelena230@gmail.com).

[**] Budimir Lutovac is with Faculty of Electrical Engineering, University of Montenegro, Montenegro (e-mail: budo@ac.me).

[***] Dragan Filipović is with Faculty of Electrical Engineering, University of Montenegro, Montenegro (e-mail: draganf@ac.me).

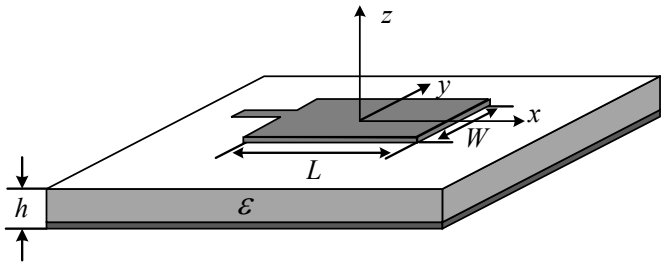

Fig. 1. Rectangular patch antenna

There are many methods of feeding a patch antenna. The most popular methods are: microstrip line (Fig. 1.), coaxial probe or aperture coupling.

Since the antenna radiates from one side of the substrate, so it is easy to feed it from the other side (the ground plane), or from the side of the element.

The advantages of the patch antennas are small size, low profile, and lightweight, conformable to planar and non planar surfaces. It demands a very little volume of the structure when mounting.

They are simple and cheap to manufacture using modern printed circuit technology. Patch antennas and their arrays are widely used in communication systems and aerial applications.

However, patch antennas have disadvantages: low efficiency, narrow bandwidth of less than 5%, low RF power due to the small separation between the radiation patch and the ground plane (not suitable for high-power applications).

There are many methods of patch antenna analysis. One of the simplest is the resonator model which treats the patch, ground plane, substrate and the feeding part as a resonator.

It is possible to have a more strict approach to the analysis of the microstrip and printed antenna of any type. It consists of solving the integral equations for the currents flowing on the antenna conductors. The integral equations can be solved by numerical methods using the computers. Once the distribution of currents is found, it is possible, as for the resonator model, to calculate all the characteristics of the antenna. These two methods are described in the literature [1] - [4].

2. RESONATOR MODEL THEORY

The resonator model (cavity model) in analyzing the patch antennas is based on the assumption that the region between the microstrip patch and ground plane is a resonance resonator bounded by ceiling and floor of electric conductors ($E_{tang} = 0$) and magnetic walls along the edge ($H_{tang} = 0$) of the conductor.

The height h of the substrate is typically a small fraction of a wavelength, such as $h = 0.05\lambda$, and the length L is of the order of 0.5λ. The structure radiates from the fringing fields that are exposed above the substrate at the edges of the patch. The fields of the lowest resonant mode (assuming $L \geq W$) are given by:

$$E_z(x) = -E_o \sin\left(\frac{\pi x}{L}\right), \text{ za } -\frac{L}{2} \le x \le \frac{L}{2}$$
$$H_y(x) = -H_o \cos\left(\frac{\pi x}{L}\right), \text{ za } -\frac{W}{2} \le x \le \frac{W}{2} \quad (1)$$

where H_0 = -jE_0/η and $\eta = \sqrt{\frac{\mu_0}{\varepsilon}}$. The origine of the coordinate system is placed in the center of the patch. It can be verified that Eqs. (1) satisfy Maxwell's equations and the boundary conditions, that is, $H_y\ (x) = 0$ at $x = \pm L/2$, provided the resonant frequency is: $\omega = \pi c/L \Rightarrow f = 0.5 \times c/L = 0.5 \times c_0 \Big/ \left(L\sqrt{\varepsilon_r}\right)$, where $c = c_0 \Big/ \sqrt{\varepsilon_r}$, $\eta = \eta_0 \Big/ \sqrt{\varepsilon_r}$, and ε_r is the relative permittivity of the dielectric substrate. It follows that the resonant microstrip length will be half-wavelength: $L = 0.5 \times \lambda / \varepsilon_r$.

Fig. 2 shows two simple models for calculating the radiation patterns of the patch antenna. The model on Fig. 2 a) assumes that the fringing fields extend over a small distance *a* around the patch sides and can be replaced with the fields E_a that are tangential to the substrate surface. The four extended edge areas around the patch serve as the effective radiating apertures.

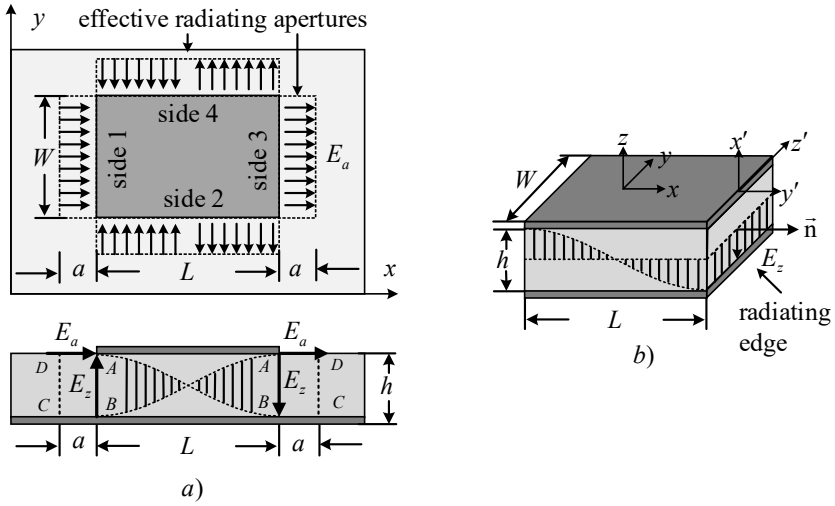

Fig 2: Aperture models for patch antenna.

The model on Fig. 2 b) assumes that the substrate is truncated beyond the extent of the patch. The four dielectric substrate walls serve now as the radiating apertures.

The only tangential aperture field on these walls is $\boldsymbol{E}_a = \overline{z}\boldsymbol{E}_z$, because the tangential magnetic fields vanish by the boundary conditions. [5]

For both models, the ground plane can be eliminated using image theory, resulting in doubling the aperture magnetic currents $\mathbf{J}_{\text{ms}}$, that is $\mathbf{J}_{ms} = -2\hat{\mathbf{n}} \times \mathbf{E}_{\mathbf{a}}$. The radiation patterns are then determined from $\mathbf{J}_{\text{ms}}$.

For the first model, the effective tangential fields can be expressed in terms of the field Ez by the relationship: $aE_a = hE_z$. This follows by requiring the vanishing of the line integrals of **E** around the loops labeled ABCD in the lower Fig. 2 a). Because $E_z = \pm E_0$ at $x = \pm L/2$, we obtain from the left and right contours:

$$\oint_{ABCD} E \cdot dl = -E_0 h + E_a a = 0, \ \oint_{ABCD} E \cdot dl = E_0 h - E_a a = 0 \Rightarrow E_a = \frac{hE_0}{a} \tag{2}$$

In obtaining these, we assumed that the electric field is nonzero only along the sides AD and AB. A similar argument for the sides 2 & 4 shows that $E_a = \pm hE_z(x)/a$. The directions of **E**a at the four sides are as shown in the figure. Thus, we have:
for sides 1 and 3:

$$E_a = \hat{x} \frac{hE_0}{a} \tag{3}$$

for sides 2 and 4:

$$E_a = \pm \hat{y} \frac{hE_z(x)}{a} = \pm \hat{y} \frac{hE_0}{a} \sin\left(\frac{\pi x}{L}\right) \tag{4}$$

The outward normal to the aperture plane is $\hat{n} = \hat{z}$ for all four sides. Therefore, the surface magnetic currents $\mathbf{J}_{ms} = -2\hat{n} \times E_a$ become:
for sides 1 i 3:

$$\mathbf{J}_{ms} = -\hat{y} \frac{2hE_0}{a} \tag{5}$$

for sides 2 i 4:

$$\mathbf{J}_{ms} = \pm \hat{x} \frac{2hE_0}{a} \sin\left(\frac{\pi x}{L}\right) \tag{6}$$

The radiated electric field is given by:

$$\mathbf{E} = jk \frac{e^{-jkr}}{4\pi r} \bar{\mathbf{r}} \times \mathbf{F}_m = jk \frac{e^{-jkr}}{4\pi r} \bar{\mathbf{r}} \times \left[\mathbf{F}_{m1} + \mathbf{F}_{m2} + \mathbf{F}_{m3} + \mathbf{F}_{m4}\right] \tag{7}$$

The vectors **F**m are the two-dimensional Fourier transforms of $\mathbf{J}_{\text{ms}}$ over the apertures:

$$\mathbf{F}_m(\theta, \phi) = \int_A \mathbf{J}_{ms}(x, y) e^{jk_x x + jk_y y} dS \tag{8}$$

The integration surfaces dS = dx dy are approximately, dS = ady for 1 & 3, and *dS* = *adx* for 2 & 4. Similarly, in the phase factor $e^{jk_x x + jk_y y}$, we must set $x = \pm L/2$ for sides 1 & 3, and $y = \mp W/2$ for sides 2 & 4. Inserting the surface magnetic currents into the Fourier integrals and combining the terms for apertures 1 & 3 and 2 & 4, we obtain:

$$\mathbf{F}_{m,13} = -\hat{y}\frac{2hE_0}{a}\int_{-W/2}^{W/2}\left(e^{-jk_x L/2} + e^{jk_x L/2}\right)e^{jk_y y}ady \tag{9}$$

$$\mathbf{F}_{m,24} = \hat{x}\frac{2hE_0}{a}\int_{-L/2}^{L/2}\left(e^{-jk_y W/2} + e^{jk_y W/2}\right)\sin\left(\frac{\pi x}{L}\right)e^{jk_x x}adx \tag{10}$$

Note that the *a* factors cancel. Using Euler's formulas and the integrals, we find the radiation vectors:

$$\mathbf{F}_{m,13} = -\hat{y}4E_0 hW\cos(\pi\nu_x)\frac{\sin(\pi\nu_y)}{\pi\nu_y} \tag{11}$$

$$\mathbf{F}_{m,24} = \hat{x}4E_0 hL\frac{4\nu_x\cos(\pi\nu_x)}{\pi(1-4\nu_x^2)}\sin(\pi\nu_y) \tag{12}$$

where we defined the normalized wavenumbers as usual:

$$\begin{aligned}\nu_x &= \frac{k_x L}{2\pi} = \frac{L}{\lambda}\sin\theta\cos\phi\\ \nu_y &= \frac{k_y W}{2\pi} = \frac{W}{\lambda}\sin\theta\sin\phi\end{aligned} \tag{13}$$

We have:

$$\begin{aligned}\hat{r}\times\hat{y} &= \hat{r}\times\left(\hat{r}\sin\theta\sin\phi + \hat{\theta}\cos\theta\sin\phi + \hat{\phi}\cos\phi\right) = \hat{\phi}\cos\theta\sin\phi - \hat{\theta}\cos\phi\\ \hat{r}\times\hat{x} &= \hat{r}\times\left(\hat{r}\sin\theta\cos\phi + \hat{\theta}\cos\theta\sin\phi - \hat{\phi}\sin\phi\right) = \hat{\phi}\cos\theta\cos\phi + \hat{\theta}\sin\phi\end{aligned} \tag{14}$$

It follows from Eq. (7) that the radiated fields from sides 1 & 3 will be:

$$E(\theta,\phi) = -jk\frac{e^{-jkr}}{4\pi r}4E_0 hW\left[\hat{\phi}\cos\theta\sin\phi - \hat{\theta}\cos\phi\right]F(\theta,\phi) \tag{15}$$

where:

$$F(\theta,\phi) = \cos(\pi\nu_x)\frac{\sin(\pi\nu_y)}{\pi\nu_y}$$

Similarly, we have for sides 2 & 4:

$$E(\theta,\phi) = jk\frac{e^{-jkr}}{4\pi r}4E_0 hL\left[\hat{\phi}\cos\theta\sin\phi + \hat{\theta}\sin\phi\right]f(\theta,\phi) \tag{16}$$

$$f(\theta,\phi)=\frac{4v_x\cos(\pi v_x)}{\pi(1-4v_x^2)}\sin(\pi v_y) \tag{17}$$

The normalized gain is found to be:

$$g(\theta,\phi)=\frac{|E(\theta,\phi)|}{|E|^2_{\max}}=\left(\cos^2\theta\sin^2\phi+\cos^2\phi\right)|F(\theta,\phi)|^2 \tag{18}$$

The corresponding expression for sides 2 & 4, although not normalized, provides a measure for the gain in that case:

$$g(\theta,\phi)=\left(\cos^2\theta\cos^2\phi+\sin^2\phi\right)|f(\theta,\phi)|^2 \tag{19}$$

The E- and H-plane gains are obtained by setting $\phi=0^\circ$ and $\phi=90^\circ$ in Eq. (18):

$$g_E(\theta)=\frac{|E_\theta|^2}{|E_\theta|^2_{max}}=|cos(\pi v_x)|^2,v_x=\frac{L}{\lambda}sin\theta \tag{20}$$

$$g_H(\theta)=\frac{|E_\phi|^2}{|E_\phi|^2_{max}}=\left|cos\theta\frac{sin(\pi v_y)}{\pi v_y}\right|^2,v_y=\frac{W}{\lambda}sin\theta \tag{21}$$

Fig. 3. shows the 3-dimensional gains from sides 1 and 3 for $W = L = 0.3371\ \lambda$, and permittivity $\varepsilon_r = 2.2$. The field strengths (square roots of the gains) are plotted to improve the visibility of the graphs.

The choice for L comes from the resonant condition $L = 0.5\lambda/\sqrt{2.2} = 0.3371\lambda$.

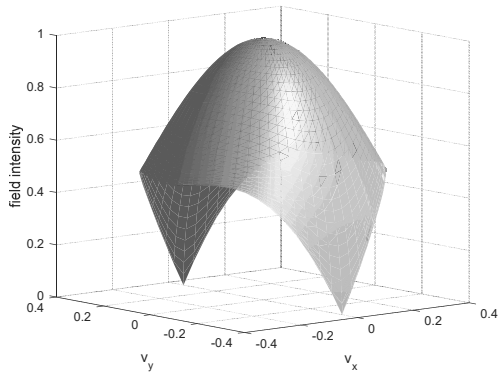

Fig. 3. Two-dimensional gain patterns from sides 1 and 3.

The gain from sides 2 and 4 vanishes along the v_x and v_y axes, when $W = L = 0.3371\ \lambda$, $\varepsilon_r = 2.2$.

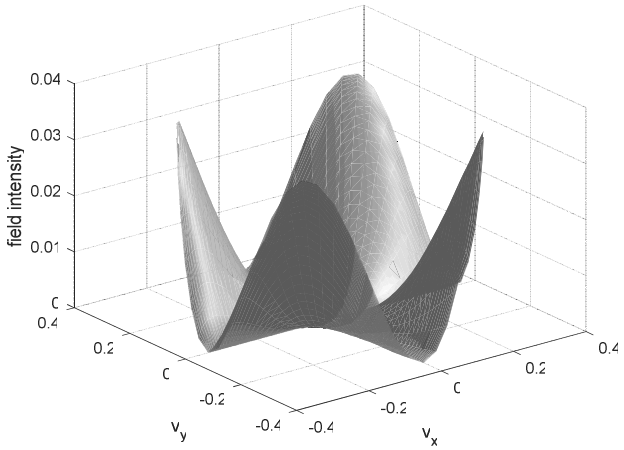

Fig. 4. Two-dimensional gain patterns from sides 2 and 4.

Most of the radiation from the patch antenna arises from sides 1 & 3. Indeed, $F(\theta,\varphi)$ has a maximum towards broadside, $\upsilon_x = \upsilon_y = 0$. Therefore, sides 2 & 4 contribute little to the total radiation, and they are usually ignored. For lengths of the order of $L = 0.3\lambda$ to $L = \lambda$, the gain function remains suppressed by 7 to 17 dB for all directions.

3. NUMERICAL RESULTS

In order to get insight how the patch antenna radiates energy out into space (or how it receives energy), the three-dimensional antenna pattern is shown on Fig 5.

It is assumed that the rectangular patch antenna (as shown in figure 1) has a resonant frequency $f_R = 2.45$ GHz. Side-lobes at E-plane appear because of the initial assumption that the patch has a finite length, and that the dielectric material substrate is shortened so that it does not cover the ground plane outside the patch. This effect is not so pronunced for radiation diagram in H-plane. The existence of the gorund plane which is covered by dielectric affects the size and phase of the picture.

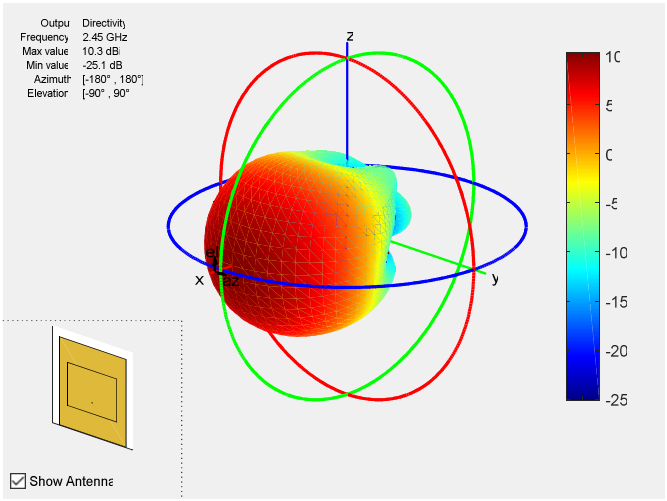

Fig. 5. Patch antenna pattern for the resonant frequency $f_r = 2.45$ GHz.

For analysis of the radiation pattern, and thus the patch antenna directivity, patch length is equal to half the wavelength, while the width is 1.5 times greater than the length, in order to improve the bandwidth. It turns out that the height of the substrate does not affect the directivity as long as it is electrically small. Fig. 6 shows the total antenna radiation in the elevation plane.

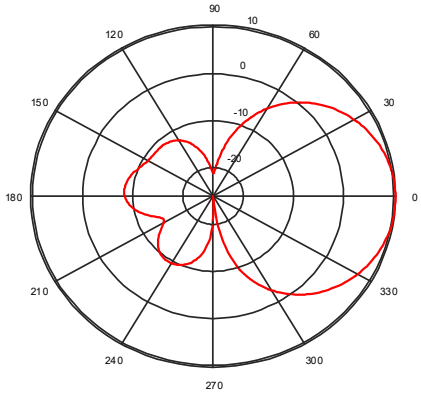

Fig. 6. Patch antenna pattern in the elevation plane for the resonant frequency $f_r = 2.45$ GHz.

The input impedance does not depend much on the height h of the substrate. It turns out that the value of the resonant input resistance can be reduced by increasing the width W of the patch. This is acceptable as long as the ratio W/L is not greater than 2, because otherwise the antenna efficiency would be reduced.

Input impedance consists of a real and an imaginary part. Imaginary part (reactance) occurs as a result of losses in metal and dielectric materials and vanishes at the resonant frequency.

Fig. 7 shows the dependence of the magnitude of the reflection coefficient S_{11} on the frequency. The purpose of this check is to confirm a good impedance match. It is typical to consider the value $S_{11} = -10\,\text{dB}$ as a threshold value for determining the antenna bandwidth.

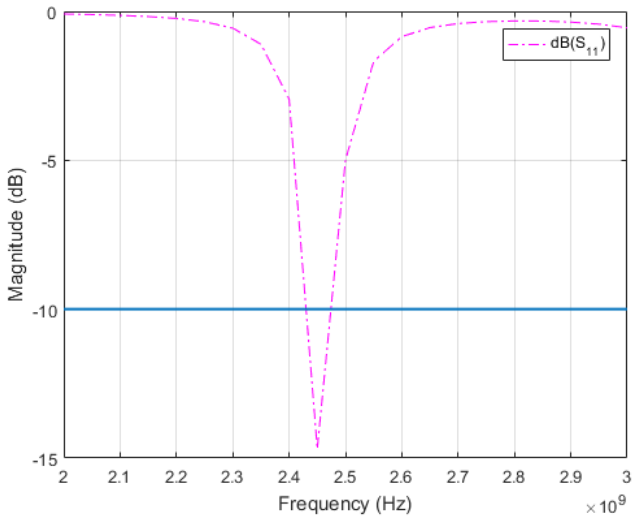

Fig. 7. S_{11} parameter

From the graph it can be seen that the reflection coefficient at the resonant frequency is equal to zero, ie, the antenna is matched to the supply line (the deep minimum at 2.45 GHz indicates a good match).

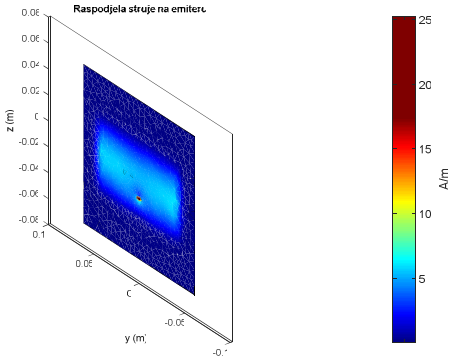

Fig. 8. Patch antenna current distribution

Finally, Fig. 8 shows the surface current density distribution on the antenna. The highest concentration of the current is in the central part of the patch, while it has a minimum at the left and right sides of the patch.

4. CONCLUSION

The paper describes the theoretical basis of the analysis using the patch antenna resonator (cavity) model. Then, the same results for directivity, reflection coefficient and current distribution are numerically obtained and graphically represented using MATLAB program package [6]. Thus, theoretical results are verified by using this software package.

5. LITERATURE

[1] Микроэлектронные устройства СВЧ, под ред. Г.И. Веселова, Высшая школа, Москва, 1988.
[2] R. Bancroft, "*Microstrip and Printed Antenna Design, Second Edition"*, SciTech Publishing, Inc. Raleigh, NC, 2009.
[3] Robert A. Sainati, "*CAD of Microstrip Antennas for Wireless Applications*", Artech House; Har/Dskt edition, January 1996.
[4] F. Alsager, "*Design and Analysis of Microstrip Patch Antenna Arrays*," Master thesis, University College of Borås, School of Engineering, January 2011
[5] Sophocles J. Orfanidis *"Electromagnetic Waves and Antennas",* Department of Electrical and Computer Engineering, Rutgers University, June 2004
[6] MATLAB, MA: The MathWorks, 2012